Title

Persistent neuropathology and behavioral deficits in a mouse model of status epilepticus induced by acute intoxication with diisopropylfluorophosphate

Authors

Calsbeek, Jonas J
González, Eduardo A
Bruun, Donald A
et al.

Publication Date

2021-12-01

DOI

10.1016/j.neuro.2021.09.001

Peer reviewed

Neurotoxicology 87 (2021) 106–119

Contents lists available at ScienceDirect

Neurotoxicology

journal homepage: www.elsevier.com/locate/neuro

Persistent neuropathology and behavioral deficits in a mouse model of *status epilepticus* induced by acute intoxication with diisopropylfluorophosphate

Jonas J. Calsbeek [a], Eduardo A. González [a], Donald A. Bruun [a], Michelle A. Guignet [a], Nycole Copping [c,d], Mallory E. Dawson [a], Alexandria J. Yu [a], Jeremy A. MacMahon [a], Naomi H. Saito [b], Danielle J. Harvey [b], Jill L. Silverman [c,d], Pamela J. Lein [a,d,*]

[a] Department of Molecular Biosciences, University of California, Davis, School of Veterinary Medicine, Davis, CA, 95616, USA
[b] Department of Public Health Sciences, University of California, Davis, School of Medicine, Davis, CA, 95616, USA
[c] Department of Psychiatry and Behavioral Sciences, School of Medicine, University of California, Davis, Sacramento, CA, 95817, USA
[d] MIND Institute, School of Medicine, University of California, Davis, Sacramento, CA, 95817, USA

ARTICLE INFO

Edited by Dr. R. Westerink

Keywords:
Acetylcholinesterase
Neurodegeneration
Neuroinflammation
Organophosphate
Seizures

ABSTRACT

Organophosphate (OP) nerve agents and pesticides are a class of neurotoxic compounds that can cause *status epilepticus* (SE), and death following acute high-dose exposures. While the standard of care for acute OP intoxication (atropine, oxime, and high-dose benzodiazepine) can prevent mortality, survivors of OP poisoning often experience long-term brain damage and cognitive deficits. Preclinical studies of acute OP intoxication have primarily used rat models to identify candidate medical countermeasures. However, the mouse offers the advantage of readily available knockout strains for mechanistic studies of acute and chronic consequences of OP-induced SE. Therefore, the main objective of this study was to determine whether a mouse model of acute diisopropylfluorophosphate (DFP) intoxication would produce acute and chronic neurotoxicity similar to that observed in rat models and humans following acute OP intoxication. Adult male C57BL/6J mice injected with DFP (9.5 mg/kg, s.c.) followed 1 min later with atropine sulfate (0.1 mg/kg, i.m.) and 2-pralidoxime (25 mg/kg, i.m.) developed behavioral and electrographic signs of SE within minutes that continued for at least 4 h. Acetylcholinesterase inhibition persisted for at least 3 d in the blood and 14 d in the brain of DFP mice relative to vehicle (VEH) controls. Immunohistochemical analyses revealed significant neurodegeneration and neuroinflammation in multiple brain regions at 1, 7, and 28 d post-exposure in the brains of DFP mice relative to VEH controls. Deficits in locomotor and home-cage behavior were observed in DFP mice at 28 d post-exposure. These findings demonstrate that this mouse model replicates many of the outcomes observed in rats and humans acutely intoxicated with OPs, suggesting the feasibility of using this model for mechanistic studies and therapeutic screening.

1. Introduction

Organophosphates (OPs) were first synthesized in the 1930s as insecticides and later discovered to kill insects via inhibition of acetylcholinesterase (AChE). AChE is conserved across species, so this discovery led to the subsequent development of OPs as G-series nerve

Abbreviations: AChE, acetylcholinesterase; DFP, diisopropylfluorophosphate; DPE, days post-exposure; FJC, FluoroJade-C; GFAP, glial fibrillary acidic protein; IBA1, ionized calcium binding adaptor molecule 1; OP, Organophosphate; SE, *status epilepticus*; SLUD, salivation, lacrimation, urination, defecation; SRS, spontaneous recurrent seizures; VEH, vehicle.

* Corresponding author at: Department of Molecular Biosciences, University of California Davis School of Veterinary Medicine, 1089 Veterinary Medicine Drive, 2009 VM3B, Davis, CA, 95616, USA.

E-mail addresses: jcalsbeek@ucdavis.edu (J.J. Calsbeek), azgonzalez@ucdavis.edu (E.A. González), dabruun@ucdavis.edu (D.A. Bruun), mguignet@ucdavis.edu (M.A. Guignet), nacopping@ucdavis.edu (N. Copping), medawson@ucdavis.edu (M.E. Dawson), aljyu@ucdavis.edu (A.J. Yu), jamacmahon@ucdavis.edu (J.A. MacMahon), nhsaito@ucdavis.edu (N.H. Saito), djharvey@ucdavis.edu (D.J. Harvey), jsilverman@ucdavis.edu (J.L. Silverman), pjlein@ucdavis.edu (P.J. Lein).

https://doi.org/10.1016/j.neuro.2021.09.001
Received 5 July 2021; Received in revised form 27 August 2021; Accepted 6 September 2021
Available online 9 September 2021

agents (e.g. sarin, soman, tabun), V-series nerve agents (e.g. VX), and Novichok agents (Adeyinka et al., 2020). While OPs were developed as chemical weapons during World War II (Munro, 1994), they were not deployed then, but were used in later conflicts such as the Iran-Iraq War and Syrian Civil War (HRW, 2021; UN, 2020). They have also been used in high profile assassinations and assassination attempts: VX agent was used to murder Kim Jong-nam in 2017 (OPCW, 2018) and Novichok agent was deployed in the attempted assassinations of Sergei and Yulia Skripal in the U.K. in 2018 (Chai et al., 2018; Haley, 2018) and Alexei Navalny in Russia in 2020 (OPCW, 2020). Consequences of acute OP intoxication in these cases included the loss of consciousness, seizures, and/or death (Figueiredo et al., 2018; Jett and Spriggs, 2020) due to the excessive accumulation of acetylcholine in cholinergic synapses throughout the peripheral and central nervous systems (Eddleston et al., 2008; Hulse et al., 2014). Moreover, each year, OP insecticides are responsible for an estimated 250,000 cases of suicide in developing nations (Eddleston et al., 2008). Thus, there is a strong interest in developing effective medical countermeasures for OP poisoning.

The current standard of care for acute OP intoxication includes the use of a muscarinic antagonist (e.g., atropine) to prevent the binding of acetylcholine (ACh) to muscarinic receptors, an oxime (e.g., 2-pralidoxime) to reactivate AChE, and a benzodiazepine (typically diazepam or midazolam) to increase GABAergic signaling in the nervous system (Eddleston et al., 2008). When injected within minutes of OP exposure,

Table 1
Summary of previous publications using mouse models of acute OP intoxication.

Strain	OP	Exposure Paradigm	SE	Neuropathology	Regions	Deficits	Citation
Male C57 (8–10 weeks)	***DFP***	***DFP (9.5 mg/kg, s.c.) AS (0.1 mg/kg, i.m.) 1 min post-DFP 2-PAM (25 mg/kg, i.m.) 1 min post-DFP***	***>4 h***	***↑ FJC at 1, 7, 28 DPE ↑ Astrogliosis at 1, 7, 28 DPE ↑ Microgliosis at 1, 7, 28 DPE***	***SS cortex Hippocampus Thalamus Piriform***	***↑ Locomotor ↑ Reactivity ↑ Anxiety ↑ Weight loss ↓ Nesting***	***Current study***
Male NIH (8 weeks)	DFP	DFP (9.93 mg/kg, s.c.) AS (3 mg/kg, i.p.) 1 min post-DFP HI-6 (50 mg/kg, i.p.) 1 min post-DFP DZP (10 mg/kg, i.p.) 80 min post-DFP	1 h	↑ astrogliosis at 1, 3 DPE ↑ microgliosis at 1, 3 DPE	CA1 CA3 DG	N/A	(Maupu, Enderlin et al. 2021)
Male NIH (7–8 weeks)	DFP	DFP (9.93 mg/kg, s.c.) AS (3 mg/kg, i.p.) 1 min post-DFP HI-6 (50 mg/kg, i.p.) 1 min post-DFP	≤11 h	↑ c-Fos at 1 HPE ↑ FJC at 1 DPE	CA1 CA3 DG	↑ ECoG	(Enderlin, Igert et al. 2020)
Male C57 (8–10 weeks)	Paraoxon	Paraoxon (0.5 mg/kg, s.c.) AS (1.5 mg/kg, i.p.) 4 min post-PXN Obidoxime (20 mg/kg, i.p.) 4 min post-PXN	>1 h	↑ thrombin activity at 10 min ↑ pERK/ERK2 levels at 10 min ↑ PAR-1/actin ratio at 30 min	CA1 CA3	↑ spike amplitude ↑ spontaneous activity (hippocampal slice)	(Golderman, Shavit-Stein et al. 2019)
Male C57 & Male NIH (8 weeks)	Paraoxon	HI-6 (50 mg/kg, i.p.) 5 min pre-PXN Paraoxon (2.4 mg/kg, s.c.)	>1 h	↑ neuronal death at 1 DPE	DG CA1 CA3 cortex amygdala	↑ spike amplitude	(Baccus, Auvin et al. 2018)
Male C57 (12–13 weeks)	Soman	HI-6 (50 mg/kg, i.p.) 5 min pre-soman Soman (172 μg/kg, s.c.) AMN (0.5 mg/kg, i.p.) 1 min post-soman DZP (5 mg/kg, i.p.) 2 h post-soman	>2 h	↑ histopathological lesionsat 43 DPE	CA1 DG piriform	↑ Mortality ↑ SRS	(McCarren, Eisen et al. 2020)
Male NIH(weight = 30 g)	Soman	HI-6 (50 mg/kg, i.p.) 5 min pre-soman Soman (172 μg/kg, s.c.) AS (10 mg/kg, i.p.) 30 or 60 min post-soman KET (25 mg/kg, i.p.) 30 or 60 min post-soman	≤1 h	↑ astrogliosis at 2, 7 DPE ↑ microgliosis at 2, 7 DPE	lateral septum piriform amygdala CA1 CA3	↑ Mortality ↑ Weight loss	(Dhote, Carpentier et al. 2012)
Male B6D (9 weeks)	Soman	Soman (110 μg/kg, s.c.) AMN (5 mg/kg, i.p.) 1 min post-soman	≥2 h	↑ neuronal death at 1, 30 DPE	amygdala	↑ Anxiety ↑ Fear Conditioning	(Collombet, Pierard et al. 2008; Coubard, Beracochea et al. 2008)
Male NIH (weight = 30 g)	Soman	HI-6 (50 mg/kg, i.p.) 5 min pre-soman Soman (172 μg/kg, s.c.)	>3 h	↑ inflammatory gene levels up to 7 DPE	cortex hippocampus cerebellum	N/A	(Dhote, Peinnequin et al. 2007)

2PAM = 2-pralidoxime; AMN = atropine methyl nitrate; AS = atropine sulfate; B6D = B6D2F1/j@rj; C57 = C57BL/6-J; DFP = diisopropylfluorophosphate; DG = dentate gyrus; DPE = days post exposure; DZP = diazepam; ECoG = electrocorticography; FJC = fluorojade C; HPE = hours post exposure; i.m. = intramuscular; i.p. = intraperitoneal; KET = ketamine; N/A = not applicable; NIH = NIH Swiss; OP = organophosphate; PXN = paraoxon; s.c. = subcutaneous; SE=*status epilepticus*; SRS = spontaneous recurrent seizures.

benzodiazepines can reduce seizure behavior and prevent death, but when their administration is delayed, they do not effectively protect against neuropathology or behavioral deficits (Masson, 2011; McDonough et al., 1999; Shih, 2000). Preclinical studies have identified potentially more effective strategies for terminating acute OP-induced *status epilepticus* (SE) (Aroniadou-Anderjaska et al., 2020; Guignet et al., 2020; Lumley et al., 2019; Marrero-Rosado et al., 2020), but there has been comparatively little progress made in identifying novel neuroprotective therapies. The latter reflects the challenge of identifying pathogenic mechanisms of chronic neurotoxicity following acute OP intoxication, which involves multiple cell types and neural circuits, as well as logistical challenges of preclinical models in which long-term survival rates can be low.

Preclinical rat models of SE induced by OPs, including diisopropylfluorophosphate (DFP), have demonstrated persistent neuropathology and/or behavioral deficits (Deshpande et al., 2010; Flannery et al., 2016; Guignet et al., 2020; Hobson et al., 2019; Pouliot et al., 2016) that recapitulate long-term effects observed in human survivors of acute OP poisoning (Jett et al., 2020). However, a mouse model of OP-induced SE would be desirable because of the availability of transgenic strains that could be leveraged to investigate pathogenic mechanisms underlying the acute and chronic neurotoxicity of acute OP intoxication. OP-induced SE has been studied in mice (see Table 1), but these studies (Baccus et al., 2018; Collombet et al., 2008; Coubard et al., 2008; Dhote et al., 2012, 2007; Enderlin et al., 2020; Golderman et al., 2019; Maupu et al., 2021; McCarren et al., 2020) have not rigorously measured the spatiotemporal progression of neuropathology at delayed times post-exposure or evaluated long-term behavioral effects. The main objective of this study was to develop a mouse model of OP-induced SE that did not require antiseizure treatment to survive with the goal of generating a model for characterizing acute and chronic neurotoxic effects with the long-term goal of using this model to investigate pathogenic mechanisms and evaluate novel therapeutics for both acute and chronic effects of acute OP intoxication. Here, we evaluate adult male C57BL/6J mice as a model of acute DFP intoxication and determine whether it exhibits chronic neuropathology and long-term behavioral deficits comparable to those observed in rat models of OP-induced SE.

2. Materials and methods

2.1. Animals

All studies involving animals conformed to the ARRIVE guidelines. Studies were designed to minimize pain and suffering and were conducted in accordance with protocols approved by the University of California, Davis Institutional Animal Care and Use Committee. Animals were housed in facilities accredited by the Association for Assessment and Accreditation of Laboratory Animal Care International. Adult male C57BL/6-J mice (8−10 weeks old; 22−33 g; Jackson Laboratory, Sacramento, CA, USA) were maintained on a 12:12 h light:dark cycle in a temperature and humidity-controlled vivarium (22 ± 2 °C; 40–50 % humidity). Mice were housed in standard plastic cages, provided chow (LabDiet, #5058) and tap water *ad libitum*, and allowed to acclimate for at least 7 d prior to experimentation. All animals used in this study were randomly assigned to experimental groups using a random number generator. Animals were group-housed (4 mice per cage) until dosed with DFP, after which animals were singly housed with additional environmental enrichment until euthanized.

2.2. Drugs and dosing paradigm

DFP was purchased from Sigma-Aldrich (St. Louis, MO, USA) and confirmed to be ~90 ± 7% pure using previously published NMR methods (Gao et al., 2016), and stored at -80 °C. DFP was prepared in sterile, ice-cold phosphate-buffered saline (PBS; 3.6 mM Na_2HPO_4, 1.4 mM NaH_2PO_4, 150 mM NaCl, pH 7.2) immediately before injection. Mice were injected with a single 100 μL bolus of DFP (Sigma-Aldrich) at 9.5–12.7 mg/kg, s.c, which corresponds to 3.3–4.4x LD_{50}, followed 1 min later by a single injection of atropine sulfate (AS; 0.1 mg/kg, i.m.; Sigma-Aldrich) and 2-pralidoxime (2-PAM; 25 mg/kg, i.m.; Sigma-Aldrich) to prevent peripheral toxicity (Fig. 1). This dosing paradigm was determined in preliminary experiments testing a range of DFP and AS doses for consistency in producing continuous seizures in DFP-exposed mice with minimal death (Supplemental material, Fig. S1). Certificates of analysis provided by the manufacturers confirmed the purity of AS (>97 %, lot #BCBM6966 V) and 2-PAM (>99 %, lot #MKCG3184). Animals in the VEH group were injected with an equivalent volume (100 μL) of sterile PBS, s.c. followed 1 min later by AS (0.1 mg/kg, i.m.) and 2-PAM (25 mg/kg, i.m.). Animals were continuously monitored for seizure behavior for 4 h after injection with DFP or VEH using a modified behavioral seizure scoring scale (Fig. 2A). At the end of the 4 h exposure period, animals were injected subcutaneously with 1 mL of 5% dextrose in sterile saline (Baxter Healthcare Co., Deerfield, IL, USA) to replace fluids lost as a result of cholinergic crisis, returned to their home cages, and given soft, moist chow daily until they resumed normal consumption of solid food and water (typically within 7 days). Body weights were measured daily after dosing with DFP, and any animal appearing weak or ill in the days following dosing with DFP were injected with 1 mL of 5% dextrose in sterile saline per day as needed.

2.3. EEG recording

A subset of mice used in this study were implanted with wireless EEG telemetry devices from Data Sciences International (HD-X02; DSI, St. Paul, MN, USA). Surgical implantation of electrodes for EEG recordings was performed in accordance with the UC Davis Rodent Survivable Surgery course. Adult mice were anesthetized using continuous isoflurane inhalation (4–5 % for induction, 1–3 % for maintenance). The head was shaved with a hair clipper and then cleaned alternately with betadine and alcohol repeated 3 times. Next, the animal was positioned in a stereotaxic frame with mouse-sized ear bars and an appropriately sized inhalation mask. A water-heated pad was put between the animal's body and the base of the stereotaxic frame to prevent hypothermia. Sterile ophthalmic ointment (Altalube; McKesson Brand, #Q187-08) was applied to the eyes to prevent dryness. Once the appropriate depth of anesthesia was confirmed using the foot pinch reflex, an approximately 0.7 inch long incision was made on the scalp along the midline from eye level to the neck level. The skin was retracted to the sides with hemostats. The periosteum was carefully scraped away from the skull to expose the bone. During the surgery, sterile saline was regularly applied to keep the surgical area hydrated. A head mount with up to 4 cortical screws, with 3 anchor crews in the skull, was implanted according to the Data Sciences International (DSI) manual. A mini drill was used to create small holes in the skull where electrodes were placed according to stereotaxic coordinates. For optimal EEG alignment, the front edge of the implant was placed 3.0–3.5 mm anterior of bregma. The tip of the implanted electrodes was located near the cortex relative to bregma using the stereotaxic coordinate system. The head mount was fixed on the skull using standard dental acrylic cement (Lang Dental Manufacturing Co Inc., Wheeling, IL, USA). The skin incision was closed with sutures, and dental cement was used to complete the skull cap. After surgery, the animals were allowed to recover for at least 7 d before experimentation, and only healthy animals continued in the study. EEG measurements were recorded untethered and only required the placement of a receiver (RPC-1; Data Sciences International, New Brighton, MN, USA) under the home cage of the animal. No other changes to the home cage environment or the well-being of the animal were required.

2.4. AChE activity

At 1, 3, 7, and 14 d after DFP or VEH exposure, subsets of mice were deeply anesthetized with 4–5 % isoflurane in medical-grade oxygen and

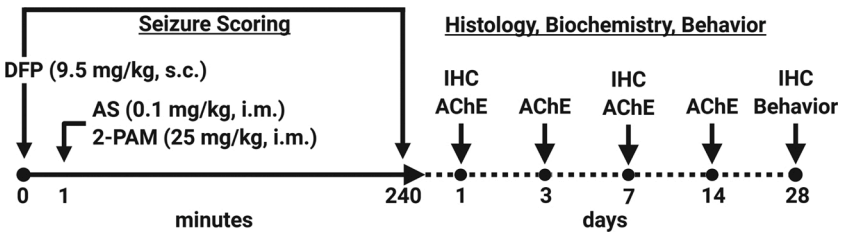

Fig. 1. Schematic of experimental design. Adult male C57BL/6-J mice were injected subcutaneously with vehicle (VEH, saline) or DFP followed one minute later by intramuscular injection of atropine sulfate (AS) and 2-pralidoxime (2-PAM). Seizure behavior was manually scored for 4 h after DFP injection, and surviving mice were randomly assigned to cohorts for histological, biochemical, or behavioral assessment at 1, 3, 7, 14, and 28 d post-exposure. AChE = acetylcholinesterase assay; DFP = diisopropylfluorophosphate; IHC = immunohistochemistry. Created with BioRender.com.

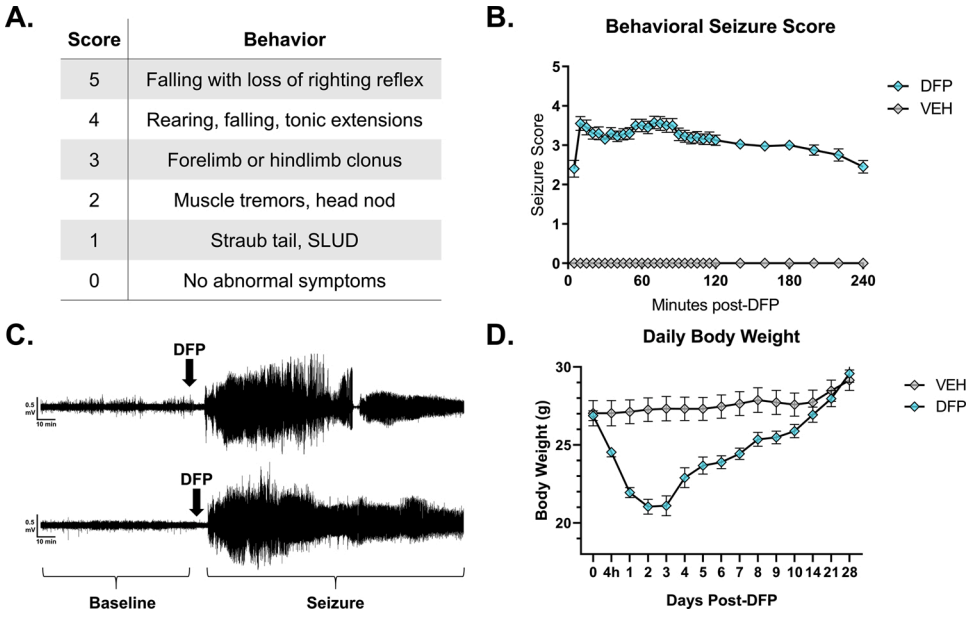

Fig. 2. Acute DFP intoxication caused robust seizure behavior, electrographic abnormalities, and weight loss in adult mice. (A) The behavioral scoring scale used to evaluate seizure behavior after DFP injection. SLUD = salivation, lacrimation, urination, defecation. (B) Resulting seizure scores for the first 4 h after DFP or VEH injection. Data points represent the mean seizure score (± SEM) for each treatment group at each time point (n = 12 mice/group). (C) Representative EEG traces of 2 individual DFP mice over 120 min of baseline and seizure recording. (D) Body weights of mice over the 28 d after injection with DFP or VEH. Data points represent the mean body weight (± SEM) for each group at each time point (n = 12 mice/group).

transcardially perfused with 25 mL ice-cold PBS (3.6 mM Na_2HPO_4, 1.4 mM NaH_2PO_4, 150 mM NaCl, pH 7.2) using a Peri-Star Pro peristaltic pump (5 mL/min). Their brains were removed and dissected to isolate the hippocampus, somatosensory cortex, and cerebellum from both hemispheres. Brain regions were flash-frozen in individual cryotubes using liquid nitrogen and stored at -80 °C until use. AChE activity was measured in the hippocampus, cortex, cerebellum, and blood using the Ellman method (Ellman et al., 1961). Tissue from each brain region was homogenized in cold sodium phosphate buffer (4 °C, 0.1 M, pH = 8.0, 1% Triton X-100; 1 ml buffer:0.1 *g* tissue), spun down in a centrifuge at 13.400xg for 1 min, and the supernatant collected. Blood plasma samples were diluted 1:25 in cold sodium phosphate buffer (4 °C, 0.1 M, pH = 8.0, 0.03 % Triton X-100) for the AChE assay. Supernatant and blood samples were plated in triplicate in a 96-well plate, and AChE activity was measured in each well using acetylthiocholine iodide (ASChI, Sigma) as the AChE substrate, and 5,5′-dithio-bis (2-nitrobenzoic acid) (DTNB, Sigma) as the colorimetric reagent. The hydrolysis of ASChI was quantified using a Synergy H1 Hybrid Plate Reader with Gen5 2.0 software (BioTek Instruments, Winooski VT, USA) by measuring changes in absorbance at 405 nm over 15 min in each well. To specifically determine AChE activity versus total cholinesterase activity, all samples were run both in the absence and presence of the butyrylcholinesterase (BChE) inhibitor, tetraisopropyl pyrophosphoramide (100 μM). AChE activity was normalized against total protein concentration with the BCA assay according to the manufacturer's directions (Pierce, Rockford, IL, USA).

2.5. Histological assessment

At 1, 7, and 28 d after exposure to DFP or VEH, mice assigned to histology cohorts were deeply anesthetized with 4–5 % isoflurane in medical-grade oxygen and transcardially perfused with 25 mL ice-cold PBS (3.6 mM Na_2HPO_4, 1.4 mM NaH_2PO_4, 150 mM NaCl, pH 7.2) using a Peri-Star Pro peristaltic pump (5 mL/min). Their brains were removed and sliced coronally into 2 mm thick sections using a mouse coronal brain matrix (Zivic Instruments, #5325; Pittsburgh, PA, USA). Sections were placed into a 24-well plate so that each well contained 1–2 brain sections submerged in 1 mL 4% (w/v) paraformaldehyde (PFA; Sigma; St. Louis, MO, USA), covered and stored at 4 °C for 18−24 h. A disposable transfer pipette was used to replace the PFA in each well with a 30 % sucrose solution. Plates were covered and stored again at 4 °C until brain tissue was fully saturated and sank to the bottom of the well. Brain sections were embedded in optimal cutting temperature medium (OCT; Fisher HealthCare; Waltham, MA, USA) and flash frozen. Blocked brain sections were stored at -80 °C until cryosectioned with a Microm HM550 cryostat (Thermo Fisher Scientific; Waltham, MA, USA). Ten micron thick coronal slices were mounted on Superfrost Plus microscope slides (Fisher HealthCare) that were stored at -80 °C until used for immunohistochemistry.

Neurodegeneration was assessed at 1, 7, and 28 d after exposure to VEH or DFP using FluoroJade C (FJC; AG325, MilliporeSigma; Burlington, MA, USA) staining. Brain sections were incubated in 0.06 % (w/v) $KMnO_4$ (Sigma) in distilled H_2O (dH_2O) for 10 min and then rinsed 3 times for 5 min in dH_2O. Slides were then incubated in FJC working solution containing FJC (0.00015 %, v/v; Cat. #AG325, lot #2301303, Millipore, Billerica, MA, USA) and DAPI (0.5 μg/mL; Invitrogen; Carlsbad, CA, USA) in 0.1 % acetic acid (v/v; Acros Organics; Geel, Belgium) in dH_2O for 10 min in the dark. Slides were rinsed 3 times for 5 min in dH_2O, then dipped in xylene (X5SK-4, Assay grade; Thermo Fisher Scientific) for 1 min and allowed to completely dry at 50 °C. Sections were

cover slipped in Permount (Thermo Fisher Scientific) and imaged at 10−20X magnification on a high content ImageXpress XLS imaging system (Molecular Devices; Sunnyvale, CA, USA). The hippocampus, piriform cortex, and thalamus of VEH and DFP mice were assessed for the number of neurons positively labeled with FJC (per mm^2) using ImageJ (NIH, USA) thresholding and cell counting by a scorer blinded to animal identification number and experimental group.

Neuroinflammation was assessed at 1, 7, and 28 d after exposure to VEH or DFP by immunohistochemistry. Sections were co-immunolabeled for GFAP and S100β to detect astrocytes or IBA1 and CD68 to detect microglia and phagocytic activity, as previously described (Guignet et al., 2020). Slides with brain sections were removed from -80 °C storage, brought to room temperature, and submerged in PBS (3.6 mM Na_2HPO_4, 1.4 mM NaH_2PO_4, 150 mM NaCl, pH 7.2) for 5 min. Antigen retrieval was performed by submerging slides in 10 mM sodium citrate buffer (pH = 6.0) and heating to 90 °C for 30 min in a vegetable steamer. After antigen retrieval, slides were washed 3 times for 5 min in PBS and then incubated in blocking buffer [PBS containing 10 % normal goat serum (v/v; Vector Laboratories), 1% bovine serum albumin (w/v; Sigma), and 0.3 % Triton X-100 (Thermo Fisher Scientific)] for 1 h at room temperature to prevent non-specific binding. Sections were next incubated in primary antibody diluted in blocking buffer at 4 °C for 18−24 h. Primary antibodies included rabbit anti-IBA1 (1:1000; 019–19741, Wako Laboratory Chemicals, Richmond, VA, USA; RRID:AB_839504), rat anti-CD68 (1:200, MCA1957, BIORAD, Hercules, CA, USA; RRID:AB_322219), mouse anti-GFAP (1:1000; 3670, Cell Signaling Technology, Danvers, MA, USA; RRID:AB_561049), and rabbit anti-S100β (1:300; ab52642, Abcam, Burlington, CA, USA; RRID:AB_882426). For negative controls, a subset of sections was incubated with blocking buffer instead of primary antibody and processed the same as the other sections. After primary incubation, sections were washed 3 times for 5 min with PBS and incubated with secondary antibody diluted in PBS with 0.3 % Triton X-100 for 1 h at room temperature. Secondary antibodies included goat anti-rabbit IgG Alexa Fluor 568 (1:1000; A11036, Life Technologies; RRID:AB_10563566), goat anti-rat IgG Alexa Fluor 488 (1:500; A11006, Thermo Fisher Scientific; RRID:AB_2534074), goat anti-mouse IgG1 Alexa Fluor 568 (1:1000; A21124, Thermo Fisher Scientific; RRID:AB_2535766), and goat anti-rabbit Alexa Fluor 488 (1:600; A11034, Thermo Fisher Scientific; RRID:AB_2576217). Sections were then washed 3 times for 5 min with PBS and cover slipped using ProLong Gold Antifade Mountant with DAPI (Invitrogen, #P36931). Fluorescent images were acquired using a high content ImageXpress XLS imaging system (Molecular Devices, Sunnyvale, CA, USA) at 10−20X magnification. Positive immunostaining was determined as fluorescent intensity that was at least twice the background fluorescence levels in the negative control samples, and all acquired images were used in the quantitative analysis. Two serial sections were analyzed for each animal in each brain region, and the total area of positive staining was averaged for each region between sections. The cortex, hippocampus, thalamus, and piriform cortex of VEH and DFP mice were analyzed using ImageJ to threshold and measure the percent area of positively labeled astrocytes and microglia by a scorer blinded to animal identification number and experimental group.

2.6. Behavioral assessment

2.6.1. Open field

At 27 d post-DFP intoxication, VEH and DFP mice were removed from their home cages and placed in a clean, empty, open field arena (48cm × 48cm x 48 cm) in a room with low lighting (~40 lx) and allowed to freely explore the arena in solitude for 30 min after the experimenter left the room. Ethovision video tracking software (EthoVision 10.1, Noldus Information Technology, Leesburg, VA, USA) was used to track the center point of the animal within the arena (3 × 3 zones) and measure the total distance traveled, average velocity, and time in center zone during the 30 min trial. After each test, the arena was cleaned with 70 % ethanol and the vapor was allowed to evaporate before the next mouse was tested.

2.6.2. Home cage reactivity

VEH and DFP mice were tested for anxiety-like behavior and hyperreactivity at 28 d post-intoxication using a modified home cage reactivity test, as previously described (Guignet et al., 2020; Raffaele et al., 1987). A blinded experimenter with gloved hands used a transfer pipette (13-711−7 M, Thermo Fisher Scientific, Waltham, MA, USA) to apply the following five stimuli, in this order: [1] a puff of air to the back; [2] light pressure to the tail base; [3] light pressure to the back; [4] light pressure to the head; [5] picking up the animal by the tail. A score between 0 and 3 was assigned to each animal to quantify the reaction to each stimulus based on the following criteria: [0] little to no reaction; [1] forward or backward movement; [2] forward or backward movement with alertness, Straub tail; [3] movement with speed, facing experimenter, or tail shake. The behavioral scores for each stimulus were added together for each animal to produce an overall reactivity score.

2.6.3. Nesting behavior

At 28 d post-DFP intoxication, the home cages of VEH and DFP mice were inspected to assess nesting behavior as determined by the animal's incorporation of a nesting pad (Nestlets, LabSupply, Fort Worth, Texas, USA) into the home cage paper nest. A blinded experimenter scored the nest in the home cage of each mouse according to the following criteria: [0] nesting pad still intact; [1] nesting pad partially shredded; [2] nesting pad fully shredded, but not incorporated into the nest; and [3] nesting pad fully shredded and incorporated into the nest.

2.7. Statistical analyses

Biochemical assay data were analyzed using one-way ANOVA with Dunnett's multiple comparisons test as performed using Prism 8.0.1 (GraphPad Software, La Jolla, CA, USA). Behavioral data were analyzed using the Mann-Whitney test as performed by Prism 8.0.1. Key outcomes considered in the histologic analyses included FJC labeling (number of cells/mm^2), % area of GFAP and S100β immunoreactivity, % area of GFAP and S100β colocalization, % area IBA1 and CD68 immunoreactivity, and % area of IBA1 and CD68 colocalization. Mixed effects models, including animal-specific random effects, were fit to assess differences between exposure groups. Primary factors of interest included exposure (DFP, VEH), region (thalamus, piriform cortex/amygdala, hippocampus, somatosensory cortex (except for FJC)), and time post-exposure (1, 7, 28 d). Interactions between the factors (treatment, region, and time point) were considered and the best model was chosen using Akaike Information Criterion. Outcomes, except for S100β and IBA1, were transformed using the natural logarithm after shifting all values by a small amount (0.1 for GFAP, GFAP/S100β colocalization, CD68 and IBA1/CD68 colocalization, and 1 for FJC) to enable the calculation for the animals with no positive staining to better meet the assumptions of the model. Contrasts for group differences, either overall or by time point or region, were constructed and tested using a Wald test. The Benjamini-Hochberg false discovery rate (FDR) was used within an outcome measure to account for multiple comparisons. Results are presented as geometric mean ratios (GMR) between exposure groups for the log-transformed outcomes and as differences between exposures for S100β and IBA1. Point estimates of the ratios or differences and 95 % confidence intervals are presented in the figures. When the confidence interval for the GMR includes 1, there is no statistical evidence of a difference between groups; similarly, when the confidence interval for the differences includes 0, there is no statistical evidence of a difference between groups. All analyses were performed using SAS (version 9.4, SAS Institute, Inc., Cary, NC, USA), graphics were created in R (version 3.6.3, R Core Team, Vienna, Austria) and alpha was set at 0.05; all reported results remained significant after the

FDR procedure.

3. Results

3.1. Acute DFP intoxication causes status epilepticus in adult male mice

Preliminary dose range-finding studies were conducted to identify doses of DFP and atropine sulfate that reliably produced *status epilepticus* (SE) with minimal death, even in the absence of antiseizure treatment (Supplemental material, Fig. S1). Administration of DFP at a dose of 9.5 mg/kg, s.c., followed immediately by administration of atropine sulfate (0.1 mg/kg, i.m.) and 2-PAM (25 mg/kg, i.m.) caused SE in 100 % of animals with > 95 % survival of all DFP-exposed animals.

Seizure behavior was quantified using a seizure severity scale to score animals during the first 4 h after injection with VEH or DFP (Fig. 2A). Scores were recorded for each animal in 5 min increments for the first 2 h after dosing, and every 20 min for the last 2 h of scoring. Symptoms of cholinergic nervous system activation, such as Straub tail and body shakes, were apparent in DFP-exposed mice within minutes of injection with DFP. Behaviors rapidly progressed to SE marked by continuous clonic or tonic seizures (seizure score ≥ 3; Fig. 2B). DFP-exposed mice (n = 12) had a mean seizure score of 3.2 ± SEM over the first 4 h of seizure scoring. VEH mice (n = 12) did not display any cholinergic signs or seizure behaviors and were assigned a seizure score of 0 for each recorded time point. To confirm that animals exhibiting seizure behavior were experiencing electrographic seizures, a subset of mice were implanted with wireless EEG recording electrodes to monitor electrical activity in the brain and muscle, respectively. Relative to baseline recordings obtained from each animal immediately prior to DFP exposure, DFP injection causes robust electrographic seizures within minutes, confirming that behavioral seizure scores corresponded to electrographic seizures in the brains of DFP mice (Fig. 2C). To monitor animal health and wellness after DFP exposure, the body weights of mice were recorded daily. Body weights of DFP mice decreased significantly compared to VEH control mice during the first 3 d post-exposure (DPE) but began to return to baseline by 4 DPE (Fig. 2D).

3.2. Acute DFP intoxication causes persistent AChE inhibition in the mouse brain

AChE activity was measured in the blood and multiple brain regions up to 14 DPE to determine the extent and duration of AChE inhibition. AChE activity was significantly inhibited in the blood for at least 3 d and in the brain for at least 14 d in DFP-intoxicated mice relative to VEH controls (Fig. 3, data represent the mean specific activity of AChE (± SEM) for VEH and DFP mice at each time point; (n = 3–9 per time point). In the somatosensory cortex, AChE activity was inhibited by 91 % on 1 DPE, 71 % on 3 DPE, 77 % on 7 DPE, and 57 % on 14 DPE relative to VEH controls. In the hippocampus, AChE was inhibited by 83 % on 1 DPE, 66 % on 3 DPE, 54 % on 7 DPE, and 41 % on 14 DPE relative to VEH controls. In the cerebellum, AChE was inhibited by 73 % on 1 DPE, 59 % on 3 DPE, 49 % on 7 DPE, and 29 % on 14 DPE, relative to VEH controls. In the blood, AChE was inhibited by 92 % on 1 DPE, 63 % on 3 DPE, 24 % on 7 DPE, and 19 % on 14 DPE, relative to VEH controls.

3.3. Acute DFP intoxication causes persistent neurodegeneration

Fluorescent images acquired using semi-automated high-content imaging revealed significantly more FJC + neurons in the hippocampus, piriform cortex, and thalamus of DFP mice relative to VEH controls at 1, 7, and 28 DPE (Fig. 4A). No FJC labeling was observed in any brain region of VEH mice at any time point, and no FJC staining was observed in the somatosensory cortex of DFP-intoxicated mice. There was no significant interaction between exposure groups and either time point or brain region. Across brain regions and time points, there was consistently more neurodegeneration observed in the DFP mice than in the VEH mice (Fig. 4B; GMR = 125.2, 95 % CI = 102.9–152.2, $p < 0.001$). Raw data used to generate this figure are provided in the supplemental material (Fig. S2).

3.4. Acute DFP intoxication causes persistent neuroinflammation

GFAP and S100β immunoreactivity were used as biomarkers to

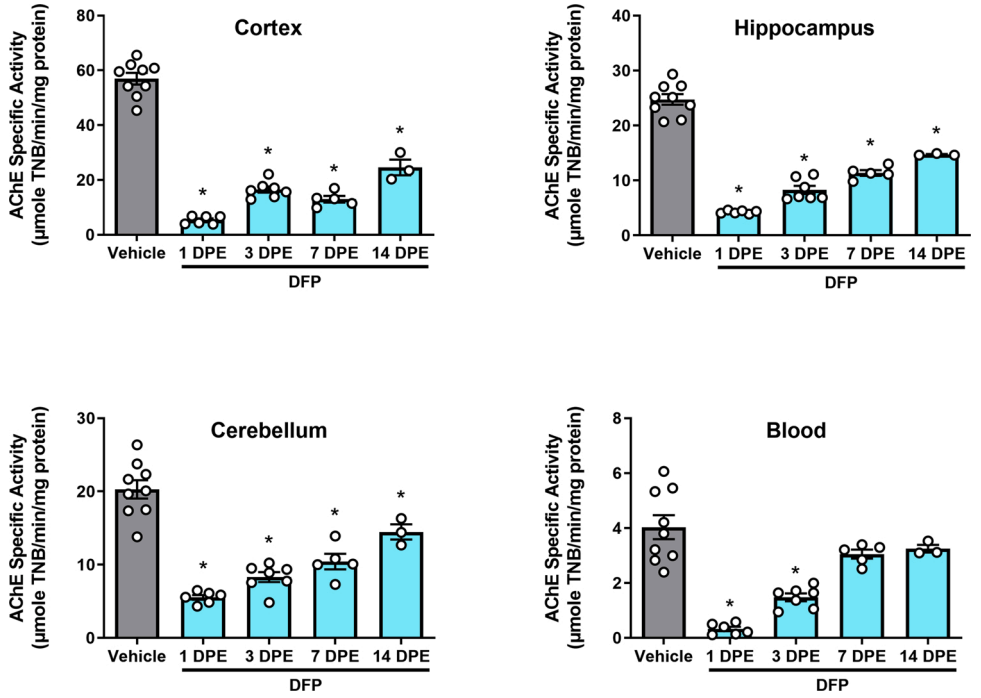

Fig. 3. Acute DFP intoxication causes persistent inhibition of AChE activity in the brain and blood. Bars reflect the mean specific activity of AChE (± SEM) for VEH and DFP mice at each time point (n = 3-9 per time point). *Significantly different from VEH at $p < 0.05$ as determined by one-way ANOVA with Dunnett's multiple comparison test. DPE = days post-exposure.

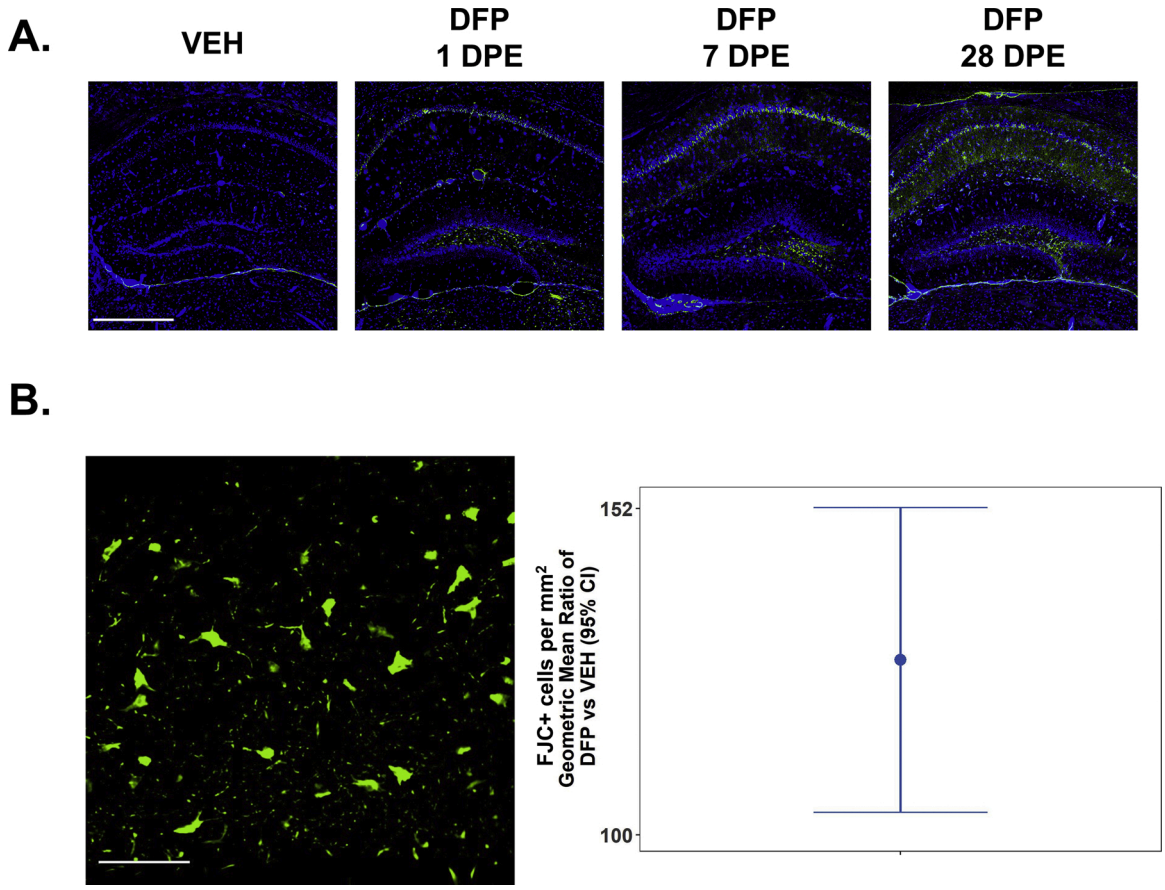

Fig. 4. Acute DFP intoxication causes persistent neurodegeneration in multiple brain regions. (A) Representative photomicrographs of the hippocampus from VEH and DFP mice stained with FluoroJade C (FJC, green) and counterstained with DAPI (blue) to label all cell nuclei. Scale bar = 1 mm. (B) Representative high magnification image of FJC + neurons from the hippocampus of DFP mice at 7 DPE. Scale bar = 50 μm. Geometric mean ratio (dot) and 95 % confidence interval (bars) of the number of FJC + cells in the hippocampus, piriform cortex, and thalamus of DFP mice relative to VEH controls at 1, 7, and 28 DPE with 95 % confidence intervals (bars). The y-axis is a log scale. Confidence intervals that do not include 1 indicate a significant difference between DFP and VEH groups. No statistically significant differences between region or DPE were found, so all brain regions and time points were collapsed. Individual data points used to generate this Fig. can be found in the supplemental material (Fig. S2).

assess reactive astrogliosis (Eng and Ghirnikar, 1994) and brain injury (Gonçalves et al., 2008) in the somatosensory cortex, hippocampus, thalamus, and piriform cortex of DFP mice (Fig. 5). GFAP is a biomarker of astrocytosis (Eng and Ghirnikar, 1994) and increased GFAP expression is associated with astrocytic responses to environmental challenge (Li et al., 2020). S100β is a biomarker of mature astrocytes (Raponi et al., 2007) and has recently garnered interest as a potential biomarker for traumatic brain injury (Oris et al., 2018). Because astrocytes undergo morphogenic changes in response to neurodegeneration or neuroinflammation (Liu et al., 2012), the area of positive immunoreactivity for these biomarkers was quantified as a readout of reactive astrogliosis. For GFAP immunolabeling, there were significant interactions between group, time point and region ($p < 0.001$) suggesting that the difference between DFP and VEH varied temporally and spatially (Fig. 5B). At 1 DPE, DFP mice had a 60 %–120 % increase in percent GFAP positive area relative to the VEH animals across all brain regions examined (cortex: GMR = 2.0, 95 % CI = 1.5–2.5, $p < 0.001$; hippocampus: GMR = 1.7, 95 % CI = 1.4–2.2, $p < 0.001$; piriform cortex: GMR = 2.2, 95 % CI = 1.6–2.9, $p < 0.001$; thalamus: GMR = 1.6, 95 % CI = 1.1–2.1, $p = 0.007$). Of the days studied, percent area of GFAP immunoreactivity in DFP animals peaked at 7 DPE, with the greatest elevation observed in the cortex (GMR = 9.6, 95 % CI = 7.2–12.7, $p < 0.001$) and piriform cortex (GMR = 6.6, 95 % CI = 5.4–8.2, $p < 0.001$) relative to the VEH mice. In these two regions, the extent of GFAP immunoreactivity decreased by 28 DPE (cortex: GMR = 1.5, 95 % CI = 1.0–2.4, $p = 0.04$; piriform cortex: GMR = 2.1, 95 % CI = 1.4–3.1, $p < 0.001$). In the hippocampus and thalamus, the increase in percent area of GFAP immunoreactivity in DFP-exposed animals relative to VEH animals observed at 7 DPE (hippocampus: GMR = 3.1, 95 % CI = 2.5–3.9, $p < 0.001$; thalamus: GMR = 3.6, 95 % CI = 2.0–6.7, $p < 0.001$) persisted at 28 DPE (hippocampus: GMR = 2.6, 95 % CI = 2.0–3.3, $p < 0.001$; thalamus: GMR = 2.8, 95 % CI = 2.0–3.8, $p < 0.001$). Raw data used to generate this figure are provided in the supplemental material (Fig. S3).

For S100β immunolabeling, there was no significant interaction between exposure group and either time point or brain region (Fig. 5C). Across brain regions and time points, there was consistently more S100β immunoreactivity observed in the DFP mice than in the VEH mice (mean difference = 5.1, 95 % CI = 3.6–6.6, $p < 0.001$). Raw data used to generate this figure are provided in the supplemental material (Fig. S3).

IBA1 and CD68 immunoreactivity were quantified as biomarkers of microglia and phagocytosis, respectively (Hendrickx et al., 2017; Ito et al., 1998), in the somatosensory cortex, hippocampus, thalamus, and piriform cortex of VEH and DFP mice (Fig. 6). The percent area of IBA1 immunoreactivity varied by brain region and time point (Fig. 6B; $p < 0.001$). In the cortex, the percent area IBA1 immunoreactivity was elevated in DFP animals compared to VEH animals at 1 DPE (mean difference = 7.6, 95 % CI = 4.4–10.7, $p < 0.001$), but not at 7 or 28 DPE. The percent area of IBA1 immunoreactivity was elevated in DFP-exposed mice relative to VEH controls across all three time points for the other three regions examined: Hippocampus: 1 DPE (diff = 7.0, 95 % CI = 3.4–10.6, $p < 0.001$), 7 DPE (diff = 12.8, 95 %CI = 7.6–18.0, $p < 0.001$), 28 DPE (diff = 7.6, 95 % CI = 4.4–10.7, $p < 0.001$); Piriform

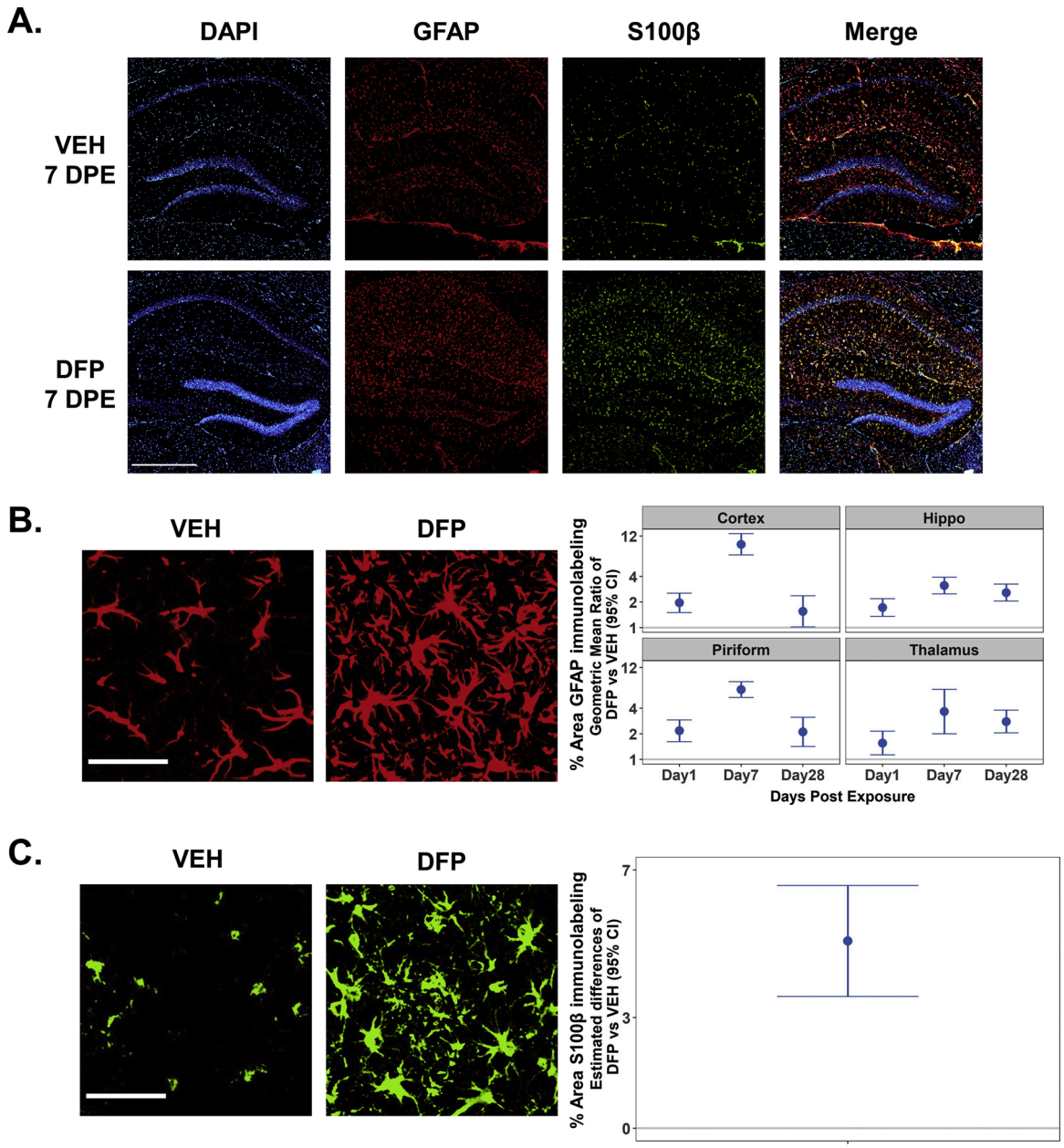

Fig. 5. DFP-induced SE caused persistent reactive astrogliosis in multiple brain regions. (A) Representative photomicrographs of the hippocampus 7 d after exposure to VEH or DFP. Coronal brain sections were immunolabeled GFAP (red) and S100β (green) to detect astrocytes, and counterstained with DAPI (blue) to detect nuclei. Scale bar = 1 mm. (B) Representative high magnification images of GFAP labeling in the hippocampus of VEH and DFP mice at 7 DPE. Scale bar = 500 μm. Geometric mean ratio (dot) of the percent area of GFAP immunoreactivity in the brain of DFP mice relative to VEH controls with 95 % confidence intervals (bars) (n = 6-8 per group). The y-axis is a log scale. Confidence intervals that do not include 1 (identified as the gray line) indicate a significant difference between DFP and VEH groups. (C) Representative high magnification images of S100β labeling in the hippocampus of VEH and DFP mice at 7 DPE. Scale bar = 500 μm. Estimated difference (dot) of the percent area of positive S100β immunolabeling in the brain of DFP mice relative to VEH controls with 95 % confidence intervals (bars) (n = 6-8 per group). Confidence intervals that do not include 0 (identified as the gray line) indicate a significant difference between DFP and VEH groups. No statistically significant differences were identified between brain regions (cortex, hippocampus, thalamus, and piriform cortex) or days post-exposure (1, 7, and 28 d), so data from all brain regions and time points were collapsed. Individual data points used to generate this figure can be found in the supplemental material (Fig. S3).

cortex: 1 DPE(diff = 9.0, 95 % CI = 5.6–12.3, $p < 0.001$), 7 DPE (diff = 11.9, 95 % CI = 6.4–17.4, $p < 0.001$), 28 DPE (diff = 6.3, 95 % CI = 0.4–12.2, $p = 0.04$); Thalamus: 1 DPE (diff = 4.0, 95 %CI = 1.0–6.9, $p = 0.01$), 7 DPE (diff = 5.1, 95 %CI = 1.1–9.0, $p = 0.01$), 28 DPE (diff = 5.4, 95 % CI = 1.1–9.7, $p = 0.01$). Raw data used to generate this figure are provided in the supplemental material (Fig. S4). The difference among groups in percent CD68 immunopositive area varied by brain region and time point (Fig. 6C; $p < 0.01$). The percent area of CD68 immunoreactivity was over 5-fold higher in DFP-exposed mice relative to VEH animals across all four brain regions and three time points that were examined ($p < 0.001$). Raw data used to generate this figure are provided in the supplemental material (Fig. S4).

For the colocalization of GFAP and S100β, there were significant interactions between group, time point and brain region ($p < 0.001$) suggesting that the difference in GFAP/S100β colocalization between DFP and VEH varied spatiotemporally (Fig. 7A). Patterns were similar to those seen for percent area of GFAP immunoreactivity with elevated levels for DFP animals compared to VEH animals across all regions 1 DPE (cortex: GMR = 2.4, 95 % CI = 1.5–3.9, $p < 0.001$; hippocampus: GMR = 2.4, 95 % CI = 1.5–3.7, $p < 0.001$; piriform cortex: GMR = 2.0,

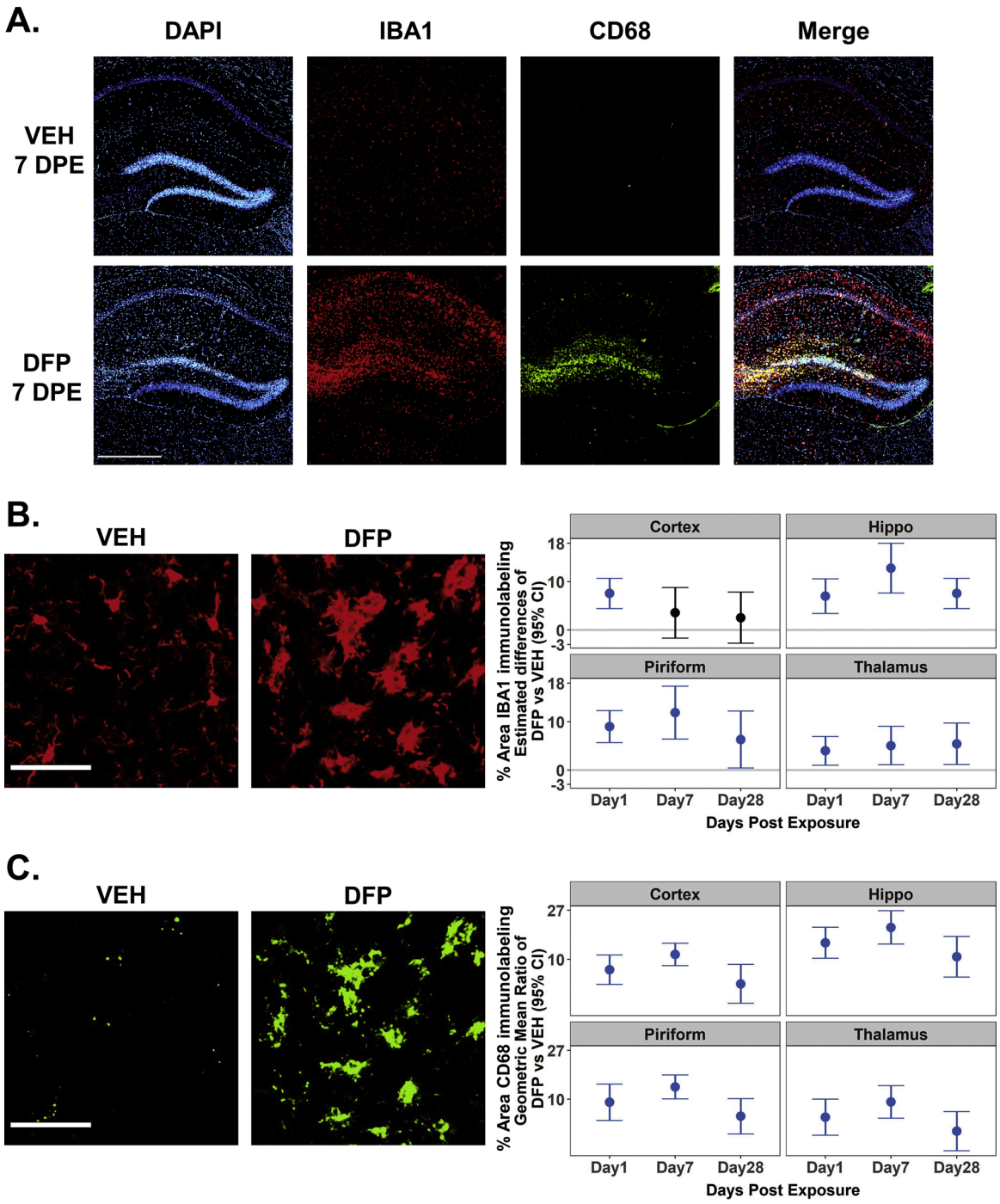

Fig. 6. DFP-induced SE caused persistent microgliosis. (A) Representative photomicrographs of the hippocampus 7 d after injection with VEH or DFP. Coronal brain sections were immunolabeled with IBA1 to detect microglia, and CD68 to detect phagocytic cells and counterstained with DAPI to detect nuclei. Bar = 1 mm. (B) Representative high magnification image of IBA1 immunoreactivity in the hippocampus of VEH and DFP mice at 7 DPE. Scale bar = 500 μm. Estimated difference (dot) of the percent area of IBA1 immunolabeling in DFP mice relative to VEH controls with 95 % confidence intervals (bars) (n = 6-8 per group). Confidence intervals that do not include 0 (identified as the gray line) indicate a significant difference between DFP and VEH groups (colored blue). (C) Representative high magnification image of CD68 immunolabeling in the hippocampus of VEH and DFP mice at 7 DPE. Scale bar = 500 μm. Geometric mean ratio (dot) of the percent area of positive CD68 immunolabeling in DFP mice relative to VEH controls with 95 % confidence intervals (bars) (n = 6-8 per group). The y-axis is a log scale. Confidence intervals that are above and do not include 1 indicate a significant difference between DFP and VEH groups. Individual data points used to generate this figure are provided in the supplemental material (Fig. S4).

95 % CI = 1.3–3.0, p = 0.002; thalamus: GMR = 2.9, 95 % CI = 1.9–4.5, p < 0.001). By 7 DPE, colocalization was highest in the cortex of DFP-exposed animals relative to VEH animals (GMR = 15.2, 95 % CI = 11.1–20.8, p < 0.001), followed by the piriform cortex (GMR = 6.2, 95 % CI = 4.6–8.5, p < 0.001), thalamus (GMR = 4.9, 95 % CI = 2.4–10.2, p < 0.001) and hippocampus (GMR = 3.7, 95 % CI = 2.6–5.4, p < 0.001). The extent of colocalization was reduced by 28 DPE in the cortex (GMR = 2.0, 95 % CI = 1.4–3.0, p < 0.001) and piriform cortex (GMR = 2.3, 95 % CI = 1.6–3.3, p < 0.001), although levels remained elevated in the hippocampus (GMR = 4.0, 95 %CI = 3.0–5.2, p < 0.001) and thalamus (GMR = 4.1, 95 %CI = 2.4–7.0, p < 0.001). The difference among groups in percent IBA1/CD68 colocalization varied by brain region and

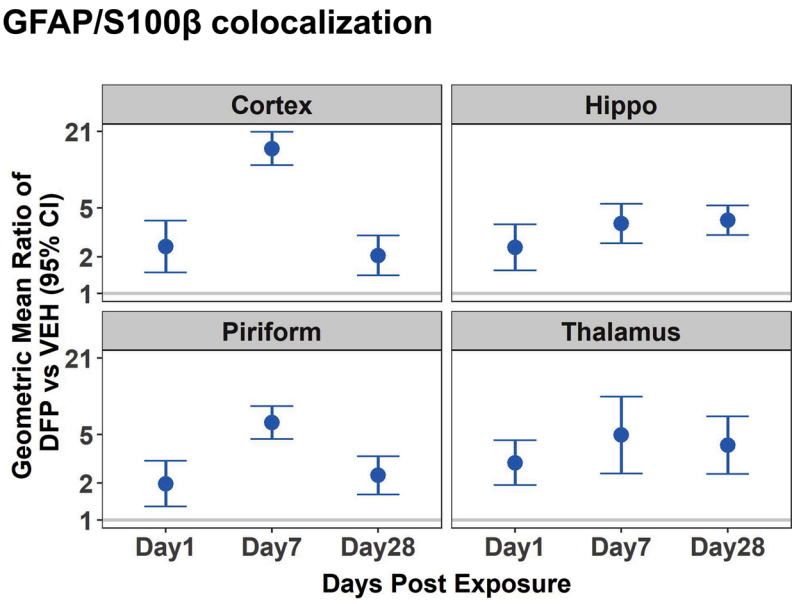

Fig. 7. Quantitative analyses of the colocalization of biomarkers for astrocytes (GFAP and S100β) and microglia (IBA1 and CD68). (A) Geometric mean ratio (dot) of the percent area of positive GFAP and positive S100β immunolabeling in the brain regions of DFP mice relative to VEH controls with 95 % confidence intervals (bars) (n = 6-8 per group). (B) Geometric mean ratio (dot) of the percent area of co-labeling for IBA1 and positive CD68 immunoreactivity in DFP mice relative to VEH controls with 95 % confidence intervals (bars) (n = 6-8 per group). In both panels, the y-axis is a log scale. Confidence intervals that do not include 1 (identified as the gray line) indicate a significant difference between DFP and VEH groups. Individual data points used to generate this figure can be found in the supplemental material (Figs. S2 and S3).

time point (Fig. 7B; $p < 0.01$). Colocalization was over 3.5 times higher in DFP exposed mice than in VEH animals across the time points and brain regions.

We determined Spearman's rank correlations between seizure score and GFAP, S100β, IBA1, and CD68 immunoreactivity by brain region and day post-exposure with 95 % confidence intervals (Fig. S5). These analyses revealed a significant positive correlation between seizure score and the extent of neuroinflammation in all brain regions at all days post-exposure.

3.5. Acute DFP intoxication causes long-term behavioral deficits

Behavioral tests were performed 28 d after exposure to VEH or DFP. At 28 DPE, deficits in locomotor activity, reactivity, and nesting behavior were observed in DFP-exposed mice (Fig. 8). In the open field test, DFP mice traveled a significantly greater distance in 30 min than VEH mice (Fig. 8A; average 18.12 m ± 2.07 compared to an average of 10.69 m ± 2.05, respectively; $p < 0.0001$). Additionally, DFP mice traveled at a significantly greater average velocity (Fig. 8A; 11.78 cm/s ± 2.26 versus 6.46 cm/s ± 1.31; $p < 0.0001$). DFP mice were also observed to spend significantly less percentage of time in the center zone of the open field arena (2.1 % ± 1.2) relative to VEH controls (Fig. 8A; 9.5 % ± 5.4; $p < 0.0001$). In the reactivity test, DFP mice were observed to be significantly more reactive to tactile stimuli than VEH mice (Fig. 8B; average reactivity score of 10.1 ± 2.92 compared to 5.63 ± 0.92, respectively; $p = 0.0035$). DFP mice were also observed to have deficits in nesting behavior relative to VEH controls. On a scale of 0–3, DFP mice averaged a score of 0.7 ± 0.95, whereas VEH mice scored an average of 3 with no nesting deficits noted (Fig. 8B; $p < 0.0001$).

4. Discussion

Our findings indicate that the mouse model of acute DFP intoxication recapitulates many of the acute and chronic neurotoxic effects observed in rat models of acute DFP intoxication. Specifically, the DFP mice exhibited: (1) acute behavioral and electrographic responses consistent with SE; (2) neurodegeneration and neuroinflammation evident at 1 DPE that persisted at 28 DPE; and (3) deficits in locomotor and home-cage behavior at 28 DPE. Thus, we believe the adult male C57BL/6-J mouse, which is the genetic background of many commercially

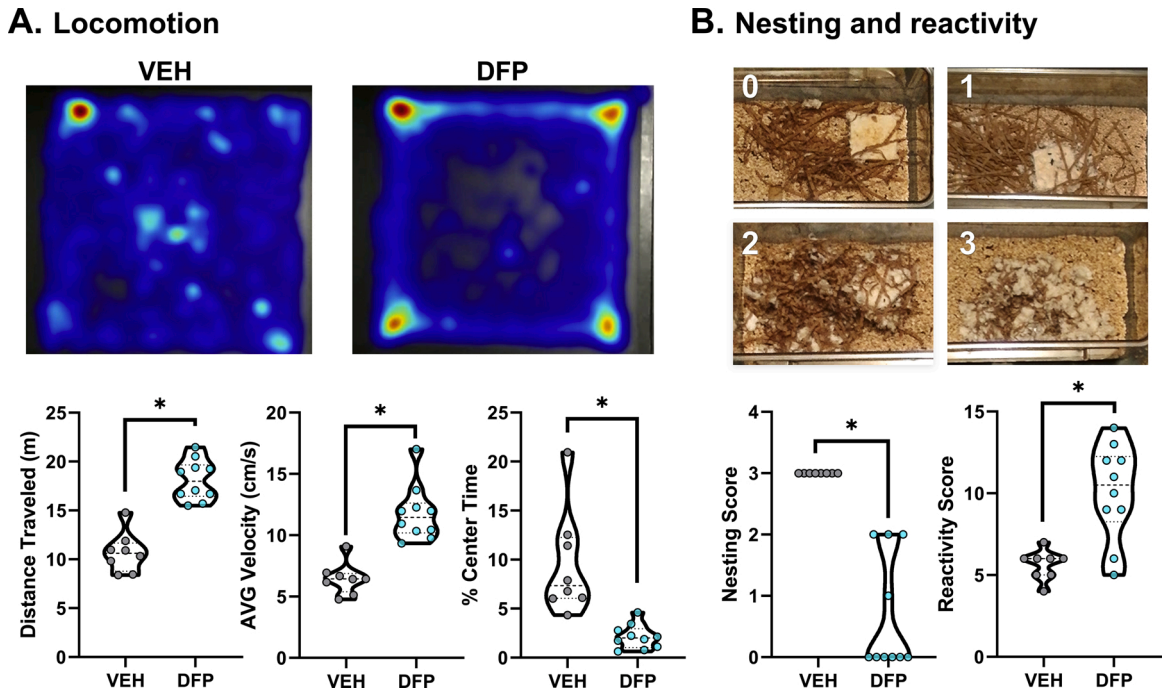

Fig. 8. Behavioral assessments of locomotion, nesting, and reactivity at 28 DPE. (A) Representative heat maps generated from 30 min in the open field assessment for a VEH and DFP mouse. Open field distance traveled (m), velocity (cm/s), and percent time spent in arena center during 30 min isolation in an open field arena. Violin plots represent the median and quartiles for distance traveled, average velocity, and percent time in center zone for VEH and DFP mice with each dot representing an individual animal (n = 8-10 per group). *Significantly different at $p < 0.0001$ as determined by an unpaired two-tailed *t*-test. (B) Representative images of the nesting pads illustrating each nesting score. Nesting and reactivity scores for VEH and DFP mice, with violin plots representing the median and quartiles and each dot representing an individual animal (n = 8-10 per group). *Significantly different at $p < 0.005$ as determined by an unpaired two-tailed *t*-test.

available transgenic mouse lines, can be used to investigate pathogenic mechanisms linking acute SE to long-term neurologic consequences and to test novel therapeutics for efficacy in mitigating chronic neurotoxic effects.

Previous studies using adult male rats to study acute DFP intoxication have demonstrated that rats exhibited signs of cholinergic crisis, including robust seizure behavior triggered within minutes of a single injection with DFP (Deshpande et al., 2010; Guignet et al., 2020; Pouliot et al., 2016). Similarly, we observed that adult male mice acutely intoxicated with DFP showed symptoms of OP poisoning within minutes after exposure, including salivation, lacrimation, urination, and defecation (SLUD) and behavioral seizures that progressed rapidly to SE lasting for at least 4 h. It should be noted that the scale used to score seizure behavior in this study was modified from the scale used in the rat model (Deshpande et al., 2010) to include specific behaviors observed in the mouse: Straub tail and tonic limb extensions. Wireless EEG recordings confirmed electrographic seizures within minutes following DFP injection and these are similar to EEG recordings of DFP-intoxicated rats (Deshpande et al., 2010; Pouliot et al., 2016). The loss of body weight in DFP mice during the first days after SE is also consistent with published observations of preclinical rat models of OP intoxication (Pessah et al., 2016; Rojas et al., 2021). Additionally, the AChE inhibition observed in the brains of DFP mice was consistent with observations in rat models of acute DFP intoxication with respect to both the percent inhibition of AChE, and the persistence of decreased AChE activity to 14 DPE (Ferchmin et al., 2014; González et al., 2020).

Prior studies in our lab of a rat model of DFP intoxication demonstrated that SE triggers progressive neuronal cell death in multiple brain regions starting at 12 h post-DFP that persists for at least 60 DPE (Sisó et al., 2017). These findings confirmed previous reports showing progressive neurodegeneration in the days following DFP-induced SE (Flannery et al., 2016; Li et al., 2011). The findings of the current study are consistent with these prior observations of rats in that DFP mice displayed persistent neurodegeneration in multiple brain regions starting as early as 1 DPE that persisted at 28 DPE. One notable difference in the spatiotemporal pattern of neurodegeneration observed in mice versus rats acutely intoxicated with DFP is that unlike rats, no FJC staining was observed in the somatosensory cortex of DFP-intoxicated mice. The reason for this difference is not known but suggests that persistent neurodegeneration is not directly linked to AChE inhibition since AChE remained significantly inhibited at 14 DPE in this brain region in the DFP mouse. Also unclear are the mechanism(s) underlying the neurodegeneration observed at delayed time points in mice. A positive correlation between seizure severity and neurodegeneration has been observed in the rat model of acute DFP intoxication (Sisó et al., 2017), suggesting that excitotoxicity influences the extent of neurodegeneration. Spontaneous recurrent seizures (SRS) have also been reported in the rat DFP model within two weeks after exposure (Guignet et al., 2020), suggesting that repeated occurrence of seizures contributes to persistent neurodegeneration. Studies are currently ongoing to determine whether mice experience SRS in the days to weeks after acute DFP intoxication.

It is well documented that DFP-induced SE triggers a robust and persistent neuroinflammatory response in the rat brain (Flannery et al., 2016; Guignet et al., 2020; Liu et al., 2012; Sisó et al., 2017) and mouse brain (Maupu et al., 2021). Consistent with these previous observations of acute OP intoxication in rat models, we observed that seizure severity, measured as the average seizure score during the first 4 h post-exposure, was positively correlated with the extent of the neuroinflammatory response, as assessed by quantitative immunohistochemical analyses of biomarkers of astrogliosis and microgliosis. We observed astrogliosis and microgliosis as early as 1 DPE that persisted at 28 DPE in multiple brain regions of DFP mice. Previous studies in the rat also demonstrated that the neuroinflammatory response induced by acute DFP intoxication varies spatiotemporally and is coincident with extensive neurodegeneration within the same brain regions (Li et al., 2011; Liu et al., 2012; Rojas et al., 2015). Thus, due to the occurrence of severe neurodegeneration in the hippocampus, piriform cortex, and thalamus of DFP

mice, it is not surprising that GFAP/S100β and IBA1/CD68 immunoreactivity remained significantly elevated in the same brain regions at 28 DPE. A significant increase in CD68 also corresponded to brain regions with elevated neurodegeneration, consistent with the suggestion that degenerating neurons trigger microglial phagocytosis. A notable difference in the spatial relationship between neurodegeneration and neuroinflammation was observed in the somatosensory cortex of DFP mice, where significant increases in GFAP/S100β and IBA1/CD68 were observed despite the absence of neurodegeneration. The reason for this discrepancy is not known, but it suggests that neurodegeneration is not the only mechanism driving a neuroinflammatory response in the brains of mice after DFP-induced SE. One possible explanation is that activated microglia in brain regions other than the somatosensory cortex triggered reactive astrogliosis and microglial activation in the somatosensory cortex through the secretion of soluble chemokines like Il-1α, TNFα, and C1q (Liddelow et al., 2017). Testing this possibility is the goal of future studies. Significantly increased S100β immunoreactivity in the brains of DFP mice are intriguing because this protein is a reliable biomarker of brain injury in survivors of OP poisoning (Yardan et al., 2013) and patients with epilepsy (Liang et al., 2019). Increased astrocytic expression of S100β has been associated with compromised blood brain barrier (BBB) integrity (Krishnan et al., 2020), suggesting that acute DFP intoxication adversely impacts the BBB. Indeed, BBB breakdown has been reported in the cortex of rats 4 days after soman-induced SE (Rojas et al., 2021), suggesting another mechanism of neuropathology in DFP mice. Future studies should investigate the potential disruption of the BBB during DFP intoxication in mice as a potential therapeutic target for OP poisoning.

It has been well established that DFP-induced SE in adult male rats causes delayed learning and memory deficits that can persist for as long as 2 months post-intoxication (Brewer et al., 2013; Flannery et al., 2016; Guignet et al., 2020). The tests used in these studies included the Morris water maze to assess spatial learning and reference memory and Pavlovian fear conditioning to assess contextual and cued learning and memory. These reports are consistent with human survivors of OP poisoning that report impaired learning and memory as one of the more common neurological consequences of acute OP intoxication (Chen, 2012; Jett et al., 2020; Okumura et al., 2005). Learning and memory tests (novel object recognition and Pavlovian fear conditioning) were performed with DFP mice at 28 DPE in this study, but the data were determined to be confounded by the observed locomotor hyperactivity in DFP mice at 28 DPE. Future studies should focus on identifying learning and memory tasks that are not confounded by hyperactivity to assess these behavioral domains in the DFP mice.

Preclinical studies of OP-induced SE in rats have also established long-term behavioral deficits in anxiety (Coubard et al., 2008) and hyperreactivity (Guignet et al., 2020), symptoms consistent with excessive arousal and post-traumatic stress disorder (Figueiredo et al., 2018; Weston, 2014). These reports are consistent with clinical literature describing the occurrence of anxiety and excessive arousal in human survivors of OP poisoning (Harrison and Ross, 2016; Levin et al., 1976; Salvi et al., 2003; Yokoyama et al., 1998). Consistent with these reports, the DFP mice exhibited signs of anxiety as indicated by increased avoidance of the center zone in the open field arena relative to VEH controls (Prut and Belzung, 2003). Elevated scores in reactivity to tactile stimuli at 7, 30, and 60 days have been previously reported in a rat model of acute DFP intoxication using an identical scoring paradigm as the current study (Guignet et al., 2020). The findings from the reactivity test in DFP mice are consistent with the rat model. Collectively, these findings that DFP-induced SE caused signs of hyperarousal and anxiety in mice at 28 DPE are consistent with the human and rat literature.

The open field test revealed that DFP mice were hyperactive as evidenced by significantly increased total distance traveled and rate of travel relative to VEH controls at 28 DPE. This locomotor deficit is inconsistent with what has been previously shown in the DFP rat model, in which no deficits in locomotor activity were observed in the open field at 1 month post-DFP (Guignet et al., 2020). The reason for the difference between models in OP-induced locomotor effects is unclear. Previous observations of hyperactivity in mice after OP exposure have been attributed to OP-induced inhibition of neuropathy target esterase (NTE; Winrow et al., 2003). Whether this explains the hyperactivity in DFP mice is not known since NTE was not assessed in the current study; however, previous studies have demonstrated that DFP can significantly inhibit NTE activity (Correll and Ehrich, 1991; Lotti et al., 1987). Additional studies are needed to quantify NTE activity in the brains of DFP mice to determine if this is a mechanism contributing to the locomotor hyperactivity in the DFP mouse model.

While decreased ability for nesting behavior has not been previously reported in DFP mice specifically, nesting deficits have been observed in several mouse models of SE induced by either pilocarpine or kainic acid that also produce hippocampal damage (Jiang et al., 2013, 2015; Jiang et al., 2019). Because brain damage or lesions in the hippocampus of mice is known to be associated with impaired nesting (Deacon, 2006), it is not surprising that DFP mice do not successfully nest at 28 DPE when the hippocampus is still exhibiting significant neurodegeneration. More long-term studies of DFP mice are needed to fully characterize the timeline of OP-induced nesting deficits in this model species relative to the persistence of hippocampal damage. Additionally, future behavioral studies using DFP mice should consider the challenges observed with locomotor hyperactivity at 28 DPE in this study, as it would be beneficial to plan for other behavioral tasks at 28 DPE that are not confounded by deficits in locomotor activity such as the sucrose preference test.

In conclusion, the findings of the current study support the hypothesis that the adult male C57BL/6J mouse DFP model recapitulates many of the acute and chronic neurotoxic effects observed in rats and humans following acute OP intoxication. Since this is the genetic background of many currently available transgenic mouse strains, this model may be ideally suited to investigate the molecular mechanisms of DFP-induced SE, neuropathology, and behavioral deficits.

An outstanding question not addressed by this study is whether strain influences acute and/or chronic effects of acute OP intoxication. This is an important consideration in light of data demonstration that the genetic background of mice can produce unique phenotypes in seizure response and behavioral deficits (Copping et al., 2019). Also not addressed in this study is the effects of acute OP intoxication on cytokine or neurotrophic factor release in the hours and days following exposure, which could illuminate the relative contribution of innate vs. adaptive immune responses in the long-term pathological and behavioral deficits observed in DFP-intoxicated mice. Ongoing studies are examining these aspects of the neuroinflammatory response in DFP mice, which would broaden our understanding of the pathogenesis of chronic neurological effects, potentially leading to the identification of novel therapeutic targets for intervention.

CRediT authorship contribution statement

Jonas J. Calsbeek: Conceptualization, Methodology, Data curation, Investigation, Writing - original draft, Visualization. **Eduardo A. González:** Methodology, Investigation, Writing - review & editing. **Donald A. Bruun:** Methodology, Investigation, Writing - review & editing. **Michelle A. Guignet:** Investigation, Writing - review & editing. **Nycole Copping:** Methodology, Investigation, Writing - review & editing. **Mallory E. Dawson:** Investigation, Writing - review & editing. **Alexandria J. Yu:** Investigation, Writing - review & editing. **Jeremy A. MacMahon:** Investigation, Writing - review & editing. **Naomi H. Saito:** Formal analysis, Writing - original draft, Writing - review & editing, Visualization. **Danielle J. Harvey:** Formal analysis, Writing - original draft, Writing - review & editing, Visualization. **Jill L. Silverman:** Resources, Writing - review & editing, Supervision. **Pamela J. Lein:** Conceptualization, Writing - review & editing, Supervision, Project administration, Funding acquisition.

Declaration of Competing Interest

The authors declare the following financial interests/personal relationships which may be considered as potential competing interests:

Pamela J. Lein reports financial support was provided by National Institute of Neurological Disorders and Stroke. Eduardo A. Gonzalez reports financial support was provided by National Institute of Neurological Disorders and Stroke. Eduardo Gonzalez reports financial support was provided by National Institute of General Medical Sciences. Michelle Guignet reports financial support was provided by National Institute of General Medical Sciences. Pamela J. Lein reports financial support was provided by National Institute of Child Health and Human Development.

Acknowledgments

The authors gratefully acknowledge Dr. Suzette Smiley-Jewell for assistance with manuscript preparation. This research was supported by the CounterACT Program, National Institutes of Health Office of the Director, and the National Institute of Neurological Disorders and Stroke (NINDS) under Grant U54 NS079202. J.J.C. was supported by a predoctoral fellowship from the UC Davis School of Veterinary Medicine; E. A.G., by predoctoral fellowships from the National Institute of Neurological Disorders and Stroke [grant number F31 NS110522] and the National Institutes of Health Initiative for Maximizing Student Development [grant number R25 GM5676520]; and M.A.G., by predoctoral fellowships from the National Institute of General Medical Sciences [grant number T32 GM099608], and the David and Dana Loury Foundation. This project used core facilities supported by the UC Davis MIND Institute Intellectual and Developmental Disabilities Research Center (Eunice Kennedy Shriver National Institute of Child Health and Human Development grant P50 HD103526). The sponsors were not involved in the study design, in the collection, analysis, or interpretation of data, in the writing of the report, or in the decision to submit the paper for publication.

Appendix A. Supplementary data

Supplementary material related to this article can be found, in the online version, at doi:https://doi.org/10.1016/j.neuro.2021.09.001.

References

Adeyinka, A., Muco, E., Pierre, L., 2020. Organophosphates. StatPearls Publishing, Treasure Island (FL).
Aroniadou-Anderjaska, V., Figueiredo, T.H., Apland, J.P., Braga, M.F., 2020. Targeting the glutamatergic system to counteract organophosphate poisoning: a novel therapeutic strategy. Neurobiol. Dis. 133, 104406.
Baccus, B., Auvin, S., Dorandeu, F., 2018. Electro-behavioral phenotype and cell injury following exposure to paraoxon-ethyl in mice: effect of the genetic background. Chem. Biol. Interact. 290, 119–125.
Brewer, K.L., Troendle, M.M., Pekman, L., Meggs, W.J., 2013. Naltrexone prevents delayed encephalopathy in rats poisoned with the sarin analogue diisopropylflurophosphate. Am. J. Emerg. Med. 31 (4), 676–679.
Chai, P.R., Hayes, B.D., Erickson, T.B., Boyer, E.W., 2018. Novichok agents: a historical, current, and toxicological perspective. Toxicol. Commun. 2 (1), 45–48.
Chen, Y., 2012. Organophosphate-induced brain damage: mechanisms, neuropsychiatric and neurological consequences, and potential therapeutic strategies. Neurotoxicology 33 (3), 391–400.
Collombet, J.M., Pierard, C., Beracochea, D., Coubard, S., Burckhart, M.F., Four, E., Masqueliez, C., Baubichon, D., Lallement, G., 2008. Long-term consequences of soman poisoning in mice Part 1. Neuropathology and neuronal regeneration in the amygdala. Behav. Brain Res. 191 (1), 88–94.
Copping, N.A., Adhikari, A., Petkova, S.P., Silverman, J.L., 2019. Genetic backgrounds have unique seizure response profiles and behavioral outcomes following convulsant administration. Epilepsy & behavior: E&B 101 (Pt A), 106547.
Correll, L., Ehrich, M., 1991. A microassay method for neurotoxic esterase determinations. Fundam. Appl. Toxicol. 16 (1), 110–116.
Coubard, S., Beracochea, D., Collombet, J.M., Philippin, J.N., Krazem, A., Liscia, P., Lallement, G., Pierard, C., 2008. Long-term consequences of soman poisoning in mice: part 2. Emotional behavior. Behav. Brain Res. 191 (1), 95–103.
Deacon, R.M., 2006. Assessing nest building in mice. Nat. Protoc. 1 (3), 1117–1119.
Deshpande, L.S., Carter, D.S., Blair, R.E., DeLorenzo, R.J., 2010. Development of a prolonged calcium plateau in hippocampal neurons in rats surviving status epilepticus induced by the organophosphate diisopropylfluorophosphate. Toxicol. Sci. 116 (2), 623–631.
Dhote, F., Peinnequin, A., Carpentier, P., Baille, V., Delacour, C., Foquin, A., Lallement, G., Dorandeu, F., 2007. Prolonged inflammatory gene response following soman-induced seizures in mice. Toxicology 238 (2-3), 166–176.
Dhote, F., Carpentier, P., Barbier, L., Peinnequin, A., Baille, V., Pernot, F., Testylier, G., Beaup, C., Foquin, A., Dorandeu, F., 2012. Combinations of ketamine and atropine are neuroprotective and reduce neuroinflammation after a toxic status epilepticus in mice. Toxicol. Appl. Pharmacol. 259 (2), 195–209.
Eddleston, M., Buckley, N.A., Eyer, P., Dawson, A.H., 2008. Management of acute organophosphorus pesticide poisoning. Lancet 371 (9612), 597–607.
Ellman, G.L., Courtney, K.D., Andres, V., Featherstone, R.M., 1961. A new and rapid colorimetric determination of acetylcholinesterase activity. Biochem. Pharmacol. 7 (2), 88–95.
Enderlin, J., Igert, A., Auvin, S., Nachon, F., Dal Bo, G., Dupuis, N., 2020. Characterization of organophosphate-induced brain injuries in a convulsive mouse model of diisopropylfluorophosphate exposure. Epilepsia 61 (6), e54–e59.
Eng, L.F., Ghirnikar, R.S., 1994. GFAP and astrogliosis. Brain Pathol. 4 (3), 229–237.
Ferchmin, P., Andino, M., Salaman, R.R., Alves, J., Velez-Roman, J., Cuadrado, B., Carrasco, M., Torres-Rivera, W., Segarra, A., Martins, A.H., 2014. 4R-cembranoid protects against diisopropylfluorophosphate-mediated neurodegeneration. Neurotoxicology 44, 80–90.
Figueiredo, T.H., Apland, J.P., Braga, M.F., Marini, A.M., 2018. Acute and long-term consequences of exposure to organophosphate nerve agents in humans. Epilepsia 59, 92–99.
Flannery, B.M., Bruun, D.A., Rowland, D.J., Banks, C.N., Austin, A.T., Kukis, D.L., Li, Y., Ford, B.D., Tancredi, D.J., Silverman, J.L., Cherry, S.R., Lein, P.J., 2016. Persistent neuroinflammation and cognitive impairment in a rat model of acute diisopropylfluorophosphate intoxication. J. Neuroinflammation 13 (1), 267.
Gao, J., Naughton, S.X., Wulff, H., Singh, V., Beck, W.D., Magrane, J., Thomas, B., Kaidery, N.A., Hernandez, C.M., Terry, A.V., 2016. Diisopropylfluorophosphate impairs the transport of membrane-bound organelles in rat cortical axons. J. Pharmacol. Exp. Ther. 356 (3), 645–655.
Golderman, V., Shavit-Stein, E., Gera, O., Chapman, J., Eisenkraft, A., Maggio, N., 2019. Thrombin and the protease-activated Receptor-1 in organophosphate-induced status epilepticus. J. Mol. Neurosci. 67 (2), 227–234.
Gonçalves, C.-A., Concli Leite, M., Nardin, P., 2008. Biological and methodological features of the measurement of S100B, a putative marker of brain injury. Clin. Biochem. 41 (10), 755–763.
González, E.A., Rindy, A.C., Guignet, M.A., Calsbeek, J.J., Bruun, D.A., Dhir, A., Andrew, P., Saito, N., Rowland, D.J., Harvey, D.J., 2020. The chemical convulsant diisopropylfluorophosphate (DFP) causes persistent neuropathology in adult male rats independent of seizure activity. Arch. Toxicol. 94 (6), 2149–2162.
Guignet, M., Dhakal, K., Flannery, B.M., Hobson, B.A., Zolkowska, D., Dhir, A., Bruun, D. A., Li, S., Wahab, A., Harvey, D.J., Silverman, J.L., Rogawski, M.A., Lein, P.J., 2020. Persistent behavior deficits, neuroinflammation, and oxidative stress in a rat model of acute organophosphate intoxication. Neurobiol. Dis. 133, 104431.
Haley, N., 2018. Remarks at an emergency UN security council briefing on chemical weapons use by russia in the United Kingdom. United States Mission to the United Nations.
Harrison, V., Ross, S.M., 2016. Anxiety and depression following cumulative low-level exposure to organophosphate pesticides. Environ. Res. 151, 528–536.
Hendrickx, D.A., van Eden, C.G., Schuurman, K.G., Hamann, J., Huitinga, I., 2017. Staining of HLA-DR, Iba1 and CD68 in human microglia reveals partially overlapping expression depending on cellular morphology and pathology. J. Neuroimmunol. 309, 12–22.
Hobson, B.A., Rowland, D.J., Siso, S., Guignet, M.A., Harmany, Z.T., Bandara, S.B., Saito, N., Harvey, D.J., Bruun, D.A., Garbow, J.R., Chaudhari, A.J., Lein, P.J., 2019. TSPO PET using [18F]PBR111 reveals persistent neuroinflammation following acute diisopropylfluorophosphate intoxication in the rat. Toxicol. Sci. 170 (2), 330–344.
HRW, 2021. The Syrian Government's Widespread and Systematic Use of Chemical Weapons. https://www.hrw.org/report/2017/05/01/death-chemicals/syrian-governments-widespread-and-systematic-use-chemical-weapons.
Hulse, E.J., Davies, J.O., Simpson, A.J., Sciuto, A.M., Eddleston, M., 2014. Respiratory complications of organophosphorus nerve agent and insecticide poisoning. Implications for respiratory and critical care. Am. J. Respir. Crit. Care Med. 190 (12), 1342–1354.
Ito, D., Imai, Y., Ohsawa, K., Nakajima, K., Fukuuchi, Y., Kohsaka, S., 1998. Microglia-specific localisation of a novel calcium binding protein, Iba1. Mol. Brain Res. 57 (1), 1–9.
Jett, D.A., Spriggs, S.M., 2020. Translational research on chemical nerve agents. Neurobiol. Dis. 133, 104335.
Jett, D.A., Sibrizzi, C.A., Blain, R.B., Hartman, P.A., Lein, P.J., Taylor, K.W., Rooney, A. A., 2020. A national toxicology program systematic review of the evidence for long-term effects after acute exposure to sarin nerve agent. Crit. Rev. Toxicol. 50 (6), 474–490.
Jiang, J., Quan, Y., Ganesh, T., Pouliot, W.A., Dudek, F.E., Dingledine, R., 2013. Inhibition of the prostaglandin receptor EP2 following status epilepticus reduces delayed mortality and brain inflammation. Proc. Natl. Acad. Sci. 110 (9), 3591–3596.
Jiang, J., Yang, M.-s., Quan, Y., Gueorguieva, P., Ganesh, T., Dingledine, R., 2015. Therapeutic window for cyclooxygenase-2 related anti-inflammatory therapy after status epilepticus. Neurobiol. Dis. 76, 126–136.

Jiang, J., Yu, Y., Kinjo, E.R., Du, Y., Nguyen, H.P., Dingledine, R., 2019. Suppressing pro-inflammatory prostaglandin signaling attenuates excitotoxicity-associated neuronal inflammation and injury. Neuropharmacology 149, 149–160.
Krishnan, A., Wu, H., Venkataraman, V., 2020. Astrocytic S100B, blood-brain barrier and neurodegenerative diseases. Glia Health Dis.
Levin, H.S., Rodnitzky, R.L., Mick, D.L., 1976. Anxiety associated with exposure to organophosphate compounds. Arch. Gen. Psychiatry 33 (2), 225–228.
Li, Y., Lein, P.J., Liu, C., Bruun, D.A., Tewolde, T., Ford, G., Ford, B.D., 2011. Spatiotemporal pattern of neuronal injury induced by DFP in rats: a model for delayed neuronal cell death following acute OP intoxication. Toxicol. Appl. Pharmacol. 253 (3), 261–269.
Li, D., Liu, X., Liu, T., Liu, H., Tong, L., Jia, S., Wang, Y.F., 2020. Neurochemical regulation of the expression and function of glial fibrillary acidic protein in astrocytes. Glia 68 (5), 878–897.
Liang, K.-G., Mu, R.-Z., Liu, Y., Jiang, D., Jia, T.-T., Huang, Y.-J., 2019. Increased serum S100B levels in patients with epilepsy: a systematic review and meta-analysis study. Front. Neurosci. 13, 456.
Liddelow, S.A., Guttenplan, K.A., Clarke, L.E., Bennett, F.C., Bohlen, C.J., Schirmer, L., Bennett, M.L., Münch, A.E., Chung, W.-S., Peterson, T.C., 2017. Neurotoxic reactive astrocytes are induced by activated microglia. Nature 541 (7638), 481–487.
Liu, C., Li, Y., Lein, P.J., Ford, B.D., 2012. Spatiotemporal patterns of GFAP upregulation in rat brain following acute intoxication with diisopropylfluorophosphate (DFP). Curr. Neurobiol. 3 (2), 90.
Lotti, M., Caroldi, S., Moretto, A., Johnson, M.K., Fish, C.J., Gopinath, C., Roberts, N.L., 1987. Central-peripheral delayed neuropathy caused by diisopropyl phosphorofluoridate (DFP): segregation of peripheral nerve and spinal cord effects using biochemical, clinical, and morphological criteria. Toxicol. Appl. Pharmacol. 88 (1), 87–96.
Lumley, L., Miller, D., Muse, W.T., Marrero-Rosado, B., de Araujo Furtado, M., Stone, M., McGuire, J., Whalley, C., 2019. Neurosteroid and benzodiazepine combination therapy reduces status epilepticus and long-term effects of whole-body sarin exposure in rats. Epilepsia Open 4 (3), 382–396.
Marrero-Rosado, B.M., de Araujo Furtado, M., Kundrick, E.R., Walker, K.A., Stone, M.F., Schultz, C.R., Nguyen, D.A., Lumley, L.A., 2020. Ketamine as adjunct to midazolam treatment following soman-induced status epilepticus reduces seizure severity, epileptogenesis, and brain pathology in plasma carboxylesterase knockout mice. Epilepsy Behav. 111, 107229.
Masson, P., 2011. Evolution of and perspectives on therapeutic approaches to nerve agent poisoning. Toxicol. Lett. 206 (1), 5–13.
Maupu, C., Enderlin, J., Igert, A., Oger, M., Auvin, S., Hassan-Abdi, R., Soussi-Yanicostas, N., Brazzolotto, X., Nachon, F., Dal Bo, G., Dupuis, N., 2021. Diisopropylfluorophosphate-induced status epilepticus drives complex glial cell phenotypes in adult male mice. Neurobiol. Dis. 152, 105276.
McCarren, H.S., Eisen, M.R., Nguyen, D.L., Dubee, P.B., Ardinger, C.E., Dunn, E.N., Haines, K.M., Santoro, A.N., Bodner, P.M., Ondeck, C.A., Honnold, C.L., McDonough, J.H., Beske, P.H., McNutt, P.M., 2020. Characterization and treatment of spontaneous recurrent seizures following nerve agent-induced status epilepticus in mice. Epilepsy Res. 162, 106320.
McDonough, J.H., Zoeffel, L.D., McMonagle, J., Copeland, T.L., Smith, C.D., Shih, T.-M., 1999. Anticonvulsant treatment of nerve agent seizures: anticholinergics versus diazepam in soman-intoxicated guinea pigs. Epilepsy Res. 38 (1), 1–14.
Munro, N., 1994. Toxicity of the organophosphate chemical warfare agents GA, GB, and VX: implications for public protection. Environ. Health Perspect. 102 (1), 18–37.
Okumura, T., Hisaoka, T., Naito, T., Isonuma, H., Okumura, S., Miura, K., Maekawa, H., Ishimatsu, S., Takasu, N., Suzuki, K., 2005. Acute and chronic effects of sarin exposure from the Tokyo subway incident. Environ. Toxicol. Pharmacol. 19 (3), 447–450.
OPCW, 2018. Statement by h.e. Ambassador Ahmad Nazri Yusof Permanent Representative of Malaysia to the OPCW at the Eighty-seventh Session of the Executive Council.
OPCW, 2020. OPCW Issues Report on Technical Assistance Requested by Germany; Alexei Navalny. https://www.opcw.org/media-centre/news/2020/10/opcw-issues-report-technical-assistance-requested-germany.
Oris, C., Pereira, B., Durif, J., Simon-Pimmel, J., Castellani, C., Manzano, S., Sapin, V., Bouvier, D., 2018. The biomarker S100B and mild traumatic brain injury: a meta-analysis. Pediatrics 141 (6).
Pessah, I.N., Rogawski, M.A., Tancredi, D.J., Wulff, H., Zolkowska, D., Bruun, D.A., Hammock, B.D., Lein, P.J., 2016. Models to identify treatments for the acute and persistent effects of seizure-inducing chemical threat agents. Ann. N. Y. Acad. Sci. 1378 (1), 124.
Pouliot, W., Bealer, S., Roach, B., Dudek, F., 2016. A rodent model of human organophosphate exposure producing status epilepticus and neuropathology. Neurotoxicology 56, 196–203.
Prut, L., Belzung, C., 2003. The open field as a paradigm to measure the effects of drugs on anxiety-like behaviors: a review. Eur. J. Pharmacol. 463 (1–3), 3–33.
Raffaele, K., Hughey, D., Wenk, G., Olton, D., Modrow, H., McDonough, J., 1987. Long-term behavioral changes in rats following organophosphonate exposure. Pharmacol. Biochem. Behav. 27 (3), 407–412.
Raponi, E., Agenes, F., Delphin, C., Assard, N., Baudier, J., Legraverend, C., Deloulme, J.-C., 2007. S100B expression defines a state in which GFAP-expressing cells lose their neural stem cell potential and acquire a more mature developmental stage. Glia 55 (2), 165–177.
Rojas, A., Ganesh, T., Lelutiu, N., Gueorguieva, P., Dingledine, R., 2015. Inhibition of the prostaglandin EP2 receptor is neuroprotective and accelerates functional recovery in a rat model of organophosphorus induced status epilepticus. Neuropharmacology 93, 15–27.
Rojas, A., McCarren, H.S., Wang, J., Wang, W., Abreu-Melon, J., Wang, S., McDonough, J.H., Dingledine, R., 2021. Comparison of neuropathology in rats following status epilepticus induced by diisopropylfluorophosphate and soman. Neurotoxicology 83, 14–27.
Salvi, R.M., Lara, D.R., Ghisolfi, E.S., Portela, L.V., Dias, R.D., Souza, D.O., 2003. Neuropsychiatric evaluation in subjects chronically exposed to organophosphate pesticides. Toxicol. Sci. 72 (2), 267–271.
Shih, T., 2000. Anticonvulsant treatment of nerve agent seizures: anticholinergics vs diazepam in soman-intoxicated guinea pigs. Epilepsy Res. 38, 114National.
Sisó, S., Hobson, B.A., Harvey, D.J., Bruun, D.A., Rowland, D.J., Garbow, J.R., Lein, P.J., 2017. Editor's highlight: spatiotemporal progression and remission of lesions in the rat brain following acute intoxication with diisopropylfluorophosphate. Toxicol. Sci. 157 (2), 330–341.
UN, 2020. Independent International Commission of Inquiry on the Syrian Arab Republic (Accessed March 14, 2021. https://www.ohchr.org/EN/HRBodies/HRC/Pages/NewsDetail.aspx?NewsID=21481&LangID=E.
Weston, C.S., 2014. Posttraumatic stress disorder: a theoretical model of the hyperarousal subtype. Front. Psychiatry 5, 37.
Winrow, C.J., Hemming, M.L., Allen, D.M., Quistad, G.B., Casida, J.E., Barlow, C., 2003. Loss of neuropathy target esterase in mice links organophosphate exposure to hyperactivity. Nat. Genet. 33 (4), 477–485.
Yardan, T., Baydin, A., Acar, E., Ulger, F., Aygun, D., Duzgun, A., Nar, R., 2013. The role of serum cholinesterase activity and S100B protein in the evaluation of organophosphate poisoning. Hum. Exp. Toxicol. 32 (10), 1081–1088.
Yokoyama, K., Araki, S., Murata, K., Nishikitani, M., Okumura, T., Ishimatsu, S., Takasu, N., White, R.F., 1998. Chronic neurobehavioral effects of Tokyo subway sarin poisoning in relation to posttraumatic stress disorder. Arch. Environ. Health Int. J. 53 (4), 249–256.